Sādhanā (2022)47:3
https://doi.org/10.1007/s12046-021-01728-8

A continuum model for predicting strain evolution in carbon fiber-reinforced composites subjected to cyclic loading

T S SADAGOAPAN[1], PARAG RAVINDRAN[1,*] and H S N MURTHY[2]

[1]Department of Mechanical Engineering, IIT Madras, Chennai 600036, India
[2]Department of Aerospace Engineering, IIT Madras, Chennai 600036, India
e-mail: sadagoapan@gmail.com; paragr@iitm.ac.in; mhsn@iitm.ac.in

MS received 14 March 2021; revised 27 July 2021; accepted 5 August 2021

Abstract. The focus of this work is on layered carbon fiber-reinforced polymers (CFRPs) subjected to cyclic loading. The response of CFRPs to cyclic loading is dictated by a variety of mechanisms that come into operation due to repetitive loading. These are quite distinct from mechanisms at play for conventional metals and alloys. Microscopic changes manifest as degradation in properties over thousands of cycles. Due to complex interactions and inherent randomness, capturing the multitude of microscopic effects and collating their effects to manifest as macroscopic changes is a difficult task. Here, the focus is on developing a continuum model which accounts for microscopic changes in an indirect, averaged manner. It is of value as it enables good estimates of material behavior without the need for detailed microscopic information. The intent is to capture the stiffness degradation over the first 10,000 cycles before there are visible changes in the material. For the material under study here, the degradation manifests in the transverse direction earlier than the longitudinal (loading) direction. The model successfully captures this behavior. The model is calibrated against experimental data from the literature.

Keywords. Carbon fiber-reinforced polymers; cyclic loading; continuum model.

1. Introduction

Composite materials, in particular carbon fiber-reinforced polymer (CFRP) composites, have a variety of industrial applications. CFRP composites consist of a polymeric matrix phase. The matrix is reinforced with strands of carbon fiber. The fibers provide additional stiffness. These composites possess a layered structure and hence they generally exhibit some form of anisotropy.

The response of CFRPs to cyclic loading is quite different from the behavior of metals. In CFRPs the damage may be as a result of matrix cracking, interfacial debonding, fiber fracture, etc. which results in changes in the material at the microscopic level. There are several factors, such as the stress ratio and loading frequency, which influence damage initiation in a composite subject to cyclic loading [1]. There are several approaches such as stiffness degradation [2, 3], residual strength degradation [4–6] and damage accumulation models available for modeling damage in composite materials [7–9]. Composites subjected to cyclic loading generally undergo three stages of damage, namely initiation, growth and failure. The present study pertains to the first stage, namely damage initiation.

Transverse matrix cracking is reported to be a dominant mode of damage initiation in laminated composites. Mall *et al* [10] studied the fatigue behavior of ceramic matrix composites reinforced with SiC fibers. They found that for crossply laminates, damage initiation manifested as transverse cracks. Van Paepegem *et al* [11, 12] proposed that Poisson's ratio could be used as a damage variable for fiber-reinforced plastics subject to fatigue loading. A degradation of Poisson's ratio measurements has been reported (see [13, 14]) in polymer/epoxy-based FRP composites under cyclic fatigue loading. Khaja Mohiddin *et al* [15] performed fatigue experiments on CFRP composites and measured strains using the digital image correlation (DIC) technique. They observed a stiffness degradation in the transverse direction much before visual delamination was perceived. They also concluded that transverse matrix cracking eventually results in failure via delamination. A continuum model that is capable of capturing the evolution of transverse strain may be of benefit in the assessment of damage initiation in a composite. The initiation of damage is of further interest in the case of polymer matrix composites owing to their viscoelastic behavior. The objective of this study is to predict the variation of strain, in particular with changes in the transverse direction (where changes are manifested earlier than changes in the loading direction), through the loading cycles during the initial

*For correspondence
Published online: 11 December 2021

phase of damage in the composite when changes are not visually apparent. The continuum model proposed here may be used to delineate the viscoelastic response due to the nature of the polymer matrix and the gradual deterioration in properties due to microscopic distress. This study does not model crack formation or propagation. It is aimed at capturing strain evolution in the early stages of damage before significant macroscopic changes are perceptible. This is particularly relevant in the case of CFRPs with a viscoelastic matrix.

In this work, a thermomechanical framework proposed by Rajagopal and Srinivasa [16] is used to develop a constitutive model to predict the variation of strain in CFRPs subject to cyclic loading. Motivated by the work of Mollica *et al* [19], a scalar measure is proposed in this paper that aids in capturing incipient damage in the material. The details of this procedure are discussed in the following section.

2. Methodology

The thermodynamic framework used in this study may be illustrated through figure 1. The reference (initial) configuration of the body is denoted by κ_R. The current configuration is denoted by κ_t. The natural configuration corresponding to the current configuration is denoted by $\kappa_{p(t)}$.

A key concept in the thermodynamic framework used here is the idea that a body may possess multiple natural configurations (natural configurations maybe thought of as stress-free configurations[1]) from which the response of the material is elastic. The natural configuration evolves as the material dissipates energy. Since there maybe an infinite number of ways in which the natural configuration can evolve, a further assumption is made. It is assumed that the natural configuration evolves in such a way that the rate of dissipation is maximized. This is a general framework for a class of viscoelastic materials, which has been used by several authors (see, e.g., [17, 18]) to model polymeric materials and other similar materials.

2.1 *Kinematic relationships*

The deformation gradient associated with the reference configuration and instantaneous natural configuration is represented by $\mathbf{F}_{\kappa_R}$and $\mathbf{F}_{\kappa_{p(t)}}$, respectively. The corresponding stretch tensors represented as $\mathbf{B}_{\kappa_R}$, $\mathbf{C}_{\kappa_R}$, $\mathbf{B}_{\kappa_{p(t)}}$and $\mathbf{C}_{\kappa_{p(t)}}$are defined as follows:

$$\mathbf{C}_{\kappa_R} := \mathbf{F}^{\mathrm{T}}_{\kappa_R}\mathbf{F}_{\kappa_R}, \tag{1}$$

[1]See Rajagopal and Srinivasa [21] for a detailed discussion on the concept of multiple natural configuration.

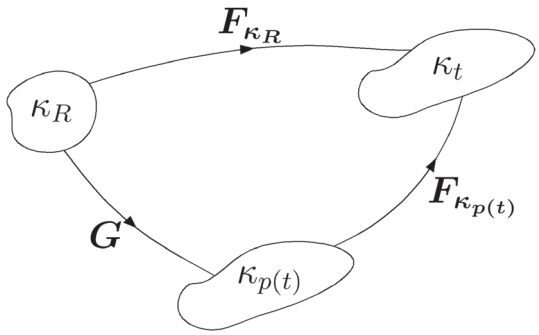

Figure 1. Schematic representation of the reference configuration (κ_R), the current configuration (κ_t) and the instantaneous natural configuration ($\kappa_{p(t)}$).

$$\mathbf{B}_{\kappa_R} := \mathbf{F}_{\kappa_R}\mathbf{F}^{\mathrm{T}}_{\kappa_R}, \tag{2}$$

$$\mathbf{C}_{\kappa_{p(t)}} := \mathbf{F}^{\mathrm{T}}_{\kappa_{p(t)}}\mathbf{F}_{\kappa_{p(t)}}, \tag{3}$$

$$\mathbf{B}_{\kappa_{p(t)}} := \mathbf{F}_{\kappa_{p(t)}}\mathbf{F}^{\mathrm{T}}_{\kappa_{p(t)}}. \tag{4}$$

$\mathbf{G}$ is defined as,

$$\mathbf{G} = \mathbf{F}^{-1}_{\kappa_{p(t)}}\mathbf{F}_{\kappa_R}. \tag{5}$$

The velocity gradient for the mapping from κ_R to κ_t and from κ_R to $\kappa_{p(t)}$, represented as $\mathbf{L}$ and $\mathbf{L}_{\kappa_{p(t)}}$, respectively, are defined as,

$$\mathbf{L} = \dot{\mathbf{F}}_{\kappa_R}\mathbf{F}^{-1}_{\kappa_R}, \tag{6}$$

$$\mathbf{L}_{\kappa_{p(t)}} = \dot{\mathbf{G}}\mathbf{G}^{-1}. \tag{7}$$

The symmetric part of the velocity gradients are defined as,

$$\mathbf{D} = \frac{1}{2}(\mathbf{L} + \mathbf{L}^{\mathrm{T}}), \tag{8}$$

$$\mathbf{D}_{\kappa_{p(t)}} = \frac{1}{2}(\mathbf{L}_{\kappa_{p(t)}} + \mathbf{L}^{\mathrm{T}}_{\kappa_{p(t)}}). \tag{9}$$

By differentiating (4) and using the above equations, it may be shown that,

$$\overset{\nabla}{\mathbf{B}}_{\kappa_{p(t)}} = -2\mathbf{F}_{\kappa_{p(t)}}\mathbf{D}_{\kappa_{p(t)}}\mathbf{F}^{\mathrm{T}}_{\kappa_{p(t)}}, \tag{10}$$

where ∇ represents the upper convected Oldroyd derivative which is defined for a tensor $\mathbf{A}$ as,

$$\overset{\nabla}{\mathbf{A}} = \dot{\mathbf{A}} - \mathbf{L}\mathbf{A} - \mathbf{A}\mathbf{L}^{\mathrm{T}}. \tag{11}$$

2.2 *Conservation laws*

The conservation laws are listed below for the sake of completeness.

2.2.1 *Conservation of mass* The conservation of mass maybe written as,

$$\frac{\partial \rho}{\partial t} + \operatorname{div}(\rho \mathbf{v}) = 0, \tag{12}$$

where ρ is the density and $\mathbf{v}$ is the velocity.

2.2.2 *Conservation of linear momentum* The conservation of linear momentum maybe written as,

$$\operatorname{div} \mathbf{T}^{\mathrm{T}} + \rho \mathbf{b} = \rho \frac{\mathrm{D}\mathbf{v}}{\mathrm{D}t}, \tag{13}$$

where $\mathbf{T}$ is the stress tensor and $\mathbf{b}$ represents the body forces. In the absence of body forces, body couples and inertial terms, the conservation of linear momentum simplifies to,

$$\operatorname{div} \mathbf{T}^{\mathrm{T}} = \mathbf{0}. \tag{14}$$

2.2.3 *Conservation of angular momentum* The conservation of linear momentum requires that,

$$\mathbf{T} = \mathbf{T}^{\mathrm{T}}. \tag{15}$$

2.2.4 *Conservation of energy* The conservation of energy demands that,

$$\rho \dot{e} + \operatorname{div} \mathbf{q} = \mathbf{T} \cdot \mathbf{D} + \rho r, \tag{16}$$

where e is the specific internal energy, $\mathbf{q}$ is the heat flux vector and r is the radiant heating.

2.2.5 *Helmholtz potential* The specific internal energy is related to Helmholtz potential through,

$$\psi = e - \eta\theta, \tag{17}$$

where ψ is the Helmholtz potential, η is the specific entropy and θ is the absolute temperature.

2.2.6 *Second law of thermodynamics* The second law of thermodynamics (in the form proposed by Green and Naghdi [22]) is,

$$\mathbf{T} \cdot \mathbf{D} - \rho \dot{\psi} - \rho \eta \dot{\theta} = \xi \geq 0, \tag{18}$$

where $\mathbf{T} \cdot \mathbf{D}$ is the stress power.

2.3 *Constitutive modeling*

The Helmholtz potential depends on the Cauchy–Green stretch tensor through its invariants. Material symmetry restrictions are imposed through additional invariants. For a transversely isotropic material, modeled through this framework, the stored energy function (ψ) and rate of dissipation (ξ) are assumed to be of the following form (it is to be noted that these are not the most general forms possible, they are chosen for ease of further use here):

$$\psi = \hat{\psi}(\mathrm{I}_{\mathbf{C}_{\kappa_R}}, \mathrm{II}_{\mathbf{C}_{\kappa_R}}, \mathrm{III}_{\mathbf{C}_{\kappa_R}}, \mathrm{J}_{\mathbf{B}_{\kappa_R}}, \mathrm{J}_{\mathbf{B}^2_{\kappa_R}}, \mathrm{I}_{\mathbf{C}_{\kappa_{p(t)}}}, \mathrm{II}_{\mathbf{C}_{\kappa_{p(t)}}}, \mathrm{III}_{\mathbf{C}_{\kappa_{p(t)}}}, \theta), \tag{19}$$

$$\xi = \hat{\xi}(\mathbf{B}_{\kappa_{p(t)}}, \mathbf{D}_{\kappa_{p(t)}}), \tag{20}$$

where I, II and III represent the principal invariants of the corresponding tensors. J is defined for any second-order tensor $\mathbf{A}$ as,

$$\mathrm{J}_{\mathbf{A}} = \mathbf{A}\mathbf{n} \cdot \mathbf{n},$$

where $\mathbf{n}$ is the preferred direction. Upon substituting the above form for the stored energy and rate of dissipation in (18) , it may be shown that,

$$\begin{aligned} \mathbf{T} \cdot \mathbf{D} - \rho \Bigg(& \frac{\partial \psi}{\partial \mathrm{I}_{\mathbf{C}_{\kappa_R}}} \dot{\mathrm{I}}_{\mathbf{C}_{\kappa_R}} + \frac{\partial \psi}{\partial \mathrm{II}_{\mathbf{C}_{\kappa_R}}} \dot{\mathrm{II}}_{\mathbf{C}_{\kappa_R}} + \frac{\partial \psi}{\partial \mathrm{III}_{\mathbf{C}_{\kappa_R}}} \dot{\mathrm{III}}_{\mathbf{C}_{\kappa_R}} \\ & + \frac{\partial \psi}{\mathrm{J}_{\mathbf{B}_{\kappa_R}}} \dot{\mathrm{J}}_{\mathbf{B}_{\kappa_R}} + \frac{\partial \psi}{\partial \mathrm{J}_{\mathbf{B}^2_{\kappa_R}}} \dot{\mathrm{J}}_{\mathbf{B}^2_{\kappa_R}} + \frac{\partial \psi}{\partial \mathrm{I}_{\mathbf{C}_{\kappa_{p(t)}}}} \dot{\mathrm{I}}_{\mathbf{C}_{\kappa_{p(t)}}} + \frac{\partial \psi}{\partial \mathrm{II}_{\mathbf{C}_{\kappa_{p(t)}}}} \dot{\mathrm{II}}_{\mathbf{C}_{\kappa_{p(t)}}} \\ & + \frac{\partial \psi}{\partial \mathrm{III}_{\mathbf{C}_{\kappa_{p(t)}}}} \dot{\mathrm{III}}_{\mathbf{C}_{\kappa_{p(t)}}} + \frac{\partial \psi}{\partial \theta} \dot{\theta} \Bigg) - \rho \eta \dot{\theta} = \xi \geq 0. \end{aligned} \tag{21}$$

The rate of dissipation (ξ) is assumed as follows:

$$\xi = 2\nu \left(\mathbf{D}_{\kappa_{p(t)}} \cdot \mathbf{B}_{\kappa_{p(t)}} \mathbf{D}_{\kappa_{p(t)}} \right)^{\beta}, \tag{22}$$

where ν and β are the model parameters. In the material under consideration here it may be expected that the inelastic deformation in the material contributes to the dissipation through the symmetric part of the rate of deformation tensor associated with $\mathbf{G}$, namely $\mathbf{D}_{\kappa_{p(t)}}$. It is noted that the chosen form is non-negative. It also goes to zero when $\mathbf{D}_{\kappa_{p(t)}}$ is zero as expected. The specific form chosen here has been successfully used to model dissipation in polymeric materials in the literature [17].

The stored energy function (ψ) is assumed to be of the form,

$$\begin{aligned} \psi = & \frac{\mu_1}{2\rho} \left[c_0 \left(\mathrm{I}_{\mathbf{C}_{\kappa_R}} - 3 \right) + c_1 \left(\mathrm{II}_{\mathbf{C}_{\kappa_R}} - 3 \right) \right] + \frac{\mu_2}{2\rho} \left(\mathrm{I}_{\mathbf{C}_{\kappa_{p(t)}}} - 3 \right) \\ & + c_2 \left(\mathrm{J}_{\mathbf{B}_{\kappa_R}} - 1 \right)^2 + c_3 \left(\mathrm{J}_{\mathbf{B}^2_{\kappa_R}} - 1 \right)^2, \end{aligned} \tag{23}$$

where μ_1, μ_2, c_0, c_1, and c_2 are the constant model parameters. The parameter c_3 is a function defined in the following manner:

$$c_3 = f(N), \text{where} N = \int_0^t \left| \mathbf{B}_{\kappa_{p(t)}}(\tau) \cdot \mathbf{D}(\tau) \right| d\tau. \tag{24}$$

N is a scalar measure that depends on the total deformation in the material. N monotonically increases with the number of cycles. This scalar has been defined in a manner that is similar to the inelastic strain path length of Mollica *et al* [19]. The function $c_3 = f(N)$ accounts for gradual changes in mechanical properties on account of accumulation of microscopic distress. It maybe shown that N is frame invariant (shown in Appendix I).

Using the above forms for stored energy and rate of dissipation in eqn. (18),

$$\begin{aligned} &2v\left(\mathbf{D}_{\kappa_{p(t)}} \cdot \mathbf{B}_{\kappa_{p(t)}} \mathbf{D}_{\kappa_{p(t)}}\right)^{\beta} = \\ &\Big[\mathbf{T} - \mu_1 \mathbf{B}_{\kappa_{p(t)}} - c_0\, \mu_2 \mathbf{B}_{\kappa_R} - 2c_1\, \mu_2 \mathbf{B}_{\kappa_R}^2 \\ &- 2c_2\left(\mathrm{J}_{\mathbf{B}_{\kappa_R}} - 1\right)\mathbf{F}_{\kappa_R}^{\mathrm{T}} \mathbf{n} \otimes \mathbf{F}_{\kappa_R}^{\mathrm{T}} \mathbf{n} - 2c_3 \\ &\left(\mathrm{J}_{\mathbf{B}_{\kappa_R}^2} - 1\right)\mathbf{B}_{\kappa_R} \mathbf{n} \otimes \mathbf{B}_{\kappa_R} \mathbf{n} \\ &- f'(N)\left(\mathrm{J}_{\mathbf{B}_{\kappa_R}^2} - 1\right)^2 \mathbf{B}_{\kappa_{p(t)}}\Big] \cdot \mathbf{D} + \mu_1\, \mathbf{B}_{\kappa_{p(t)}} \cdot \mathbf{D}_{\kappa_{p(t)}}. \end{aligned} \tag{25}$$

The following constitutive relation for stress is obtained as a sufficient condition to partially satisfy eqn. (25)

$$\begin{aligned} \mathbf{T} = &-p_0 \mathbf{I} + \overline{\mu}_1 \mathbf{B}_{\kappa_{p(t)}} + c_0\, \mu_2\, \mathbf{B}_{\kappa_R} + 2c_1\, \mu_2\, \mathbf{B}_{\kappa_R}^2 \\ &+ 2c_2\left(\mathrm{J}_{\mathbf{B}_{\kappa_R}} - 1\right)\mathbf{F}_{\kappa_R}^{\mathrm{T}} \mathbf{n} \otimes \mathbf{F}_{\kappa_R}^{\mathrm{T}} \mathbf{n} \\ &+ 2c_3\left(\mathrm{J}_{\mathbf{B}_{\kappa_R}^2} - 1\right)\mathbf{B}_{\kappa_R} \mathbf{n} \otimes \mathbf{B}_{\kappa_R} \mathbf{n}, \end{aligned} \tag{26}$$

where

$$\overline{\mu}_1 = \mu_1 + f'(N)\left(\mathrm{J}_{\mathbf{B}_{\kappa_R}^2} - 1\right)^2,$$

and p_0 is the Lagrange multiplier introduced to enforce the constraint of incompressibility. The following form for c_3 is assumed:

$$c_3(N) = \frac{p}{(N+s)^r} + q, \text{where} N = \int_0^t \left| \mathbf{B}_{\kappa_{p(t)}}(\tau) \cdot \mathbf{D}(\tau) \right| d\tau, \tag{27}$$

where p, q, r and s are the parameters. As the number of cycles increases, c_3 decreases, the material softens and the transverse strain increases. In order to capture this behavior, the above form for c_3 has been chosen.

The evolution of instantaneous natural configuration $\mathbf{B}_{\kappa_{p(t)}}$ over time is required to characterize the response of the material. This is obtained by constrained maximization of the rate of dissipation function subject to constraints of incompressibility and the reduced dissipation equation eqn. (25). The augmented function is written as,

$$\begin{aligned} \phi = &\xi + \lambda_1 \left[2v\left(\mathbf{D}_{\kappa_{\mathbf{p}(\mathbf{t})}} \cdot \mathbf{B}_{\kappa_{\mathbf{p}(\mathbf{t})}} \mathbf{D}_{\kappa_{\mathbf{p}(\mathbf{t})}}\right)^{\beta} - \mu_1\, \mathbf{B}_{\kappa_{p(t)}} \cdot D_{\kappa_{p(t)}}\right] \\ &+ \lambda_2 (\mathbf{D}_{\kappa_{\mathbf{p}(\mathbf{t})}} \cdot \mathbf{I}), \end{aligned} \tag{28}$$

where λ_1 and λ_2 are the Lagrange multipliers for the constrained maximization. By differentiating (28) with respect to $\mathbf{D}_{\kappa_{\mathbf{p}(\mathbf{t})}}$ and equating it to zero, the following equation is obtained:

$$\overset{\nabla}{\mathbf{B}}_{\kappa_{p(t)}} = -2\left(\frac{\mu_1}{2v}\right)^{\frac{1}{(2\beta-1)}} \left[\mathrm{I}_{\mathbf{B}_{\kappa_{p(t)}}} - \frac{9}{\mathrm{I}_{\mathbf{B}_{\kappa_{p(t)}}^{-1}}}\right]^{\frac{(1-\beta)}{2\beta-1}} \left[\mathbf{B}_{\kappa_{p(t)}} - \frac{3}{\mathrm{I}_{\mathbf{B}_{\kappa_{p(t)}}^{-1}}} \mathbf{I}\right]. \tag{29}$$

λ_1 is given by,

$$\lambda_1 = \frac{2\beta}{1-2\beta}. \tag{30}$$

λ_2 is given by,

$$\lambda_2 = \frac{3\lambda_1 \mu_1}{tr\, \mathbf{B}_{\kappa_{p(t)}}^{-1}}. \tag{31}$$

2.4 *Application of the model to uniaxial loading*

The model predictions are compared against experimental data reported by Khaja Mohiddin [20]. They conducted cyclic uniaxial loading experiments on laminated composite specimens (75 mm × 25 mm × 2.73 mm) consisting of 17 laminae with an ultimate tensile strength (σ_{ult}) of 677 MPa. The epoxy resin (Epolam 2063) matrix was reinforced with carbon fibers. As shown in figure 2, the composite was loaded along the Z direction and the laminae were stacked along the Y-axis with a stacking sequence $[0, \pm 45, 90]_s$. This layup sequence produces a quasi-isotropic laminate. For modeling purposes, this is assumed to produce a transversely isotropic material with one preferred direction along layup direction i.e., the Y-axis.

The experiments consisted of low cycle fatigue for a given stress ratio, $R = 0.5$ (cyclic tension–tension loading) and load frequency, $f = 1$ Hz. The data broadly consisted of two sets corresponding to two different stress levels: set 1 corresponding to $\sigma_{\max} = 90\%\ \sigma_{ult}$ and those of set 2 being $\sigma_{\max} = 95\%\ \sigma_{ult}$. The input load was measured with the help of a load cell and strains were measured through DIC. In order to model this data a semi-inverse approach is employed here.

The current configuration $\mathbf{x}$ is defined by coordinates (x, y, z) and the reference configuration $\mathbf{X}$ is defined by coordinates (X, Y, Z). For a homogeneous, axial extension, the motion is assumed to be,

$$x = \lambda_1(t)X, \qquad y = \lambda_2(t)Y, \qquad z = \frac{1}{\lambda_1(t)\lambda_2(t)}Z, \tag{32}$$

where $\lambda_1(t)$ and $\lambda_2(t)$ are the stretch ratios along the X and Y directions, respectively.

The deformation gradient $\mathbf{F}_{\kappa_R}$ and the left Cauchy–Green stretch tensor $\mathbf{B}_{\kappa_R}$ are easily computed. The form for $\mathbf{B}_{\kappa_{p(t)}}$ is assumed to be similar to $\mathbf{B}_{\kappa_R}$. $B_1(t)$ and $B_2(t)$ are unknown scalar functions. The choice of the form for $\mathbf{B}_{\kappa_{p(t)}}$ is an assumption. Its justification lies in the physically reasonable solutions that are obtained with this choice. Thus,

$$\mathbf{F}_{\kappa_R} = \mathrm{diag}\left(\lambda_1, \lambda_2, \frac{1}{\lambda_1\lambda_2}\right), \tag{33}$$

$$\mathbf{B}_{\kappa_R} = \mathrm{diag}\left(\lambda_1^2, \lambda_2^2, \frac{1}{\lambda_1^2\lambda_2^2}\right), \tag{34}$$

$$\mathbf{B}_{\kappa_{p(t)}} = \mathrm{diag}\left(B_1, B_2, \frac{1}{B_1B_2}\right). \tag{35}$$

The stress is obtained from the constitutive eqn. (26). The conservation of linear momentum eqn. (14) is solved using the traction free conditions on the lateral faces:

$$T_{xx} = -p_0 + \overline{\mu}_1 B_1 + c_0\mu_2\lambda_1^2 + 2c_1\mu_2\lambda_1^4 = 0, \tag{36}$$

$$\begin{aligned} T_{yy} = -p_0 + \overline{\mu}_1 B_2 + c_0\mu_2\lambda_2^2 + 2c_2(\lambda_2^2-1)\lambda_2^2 \\ + 2c_1\mu_2\lambda_2^4 + 2c_3(\lambda_2^4-1)\lambda_2^4 = 0, \end{aligned} \tag{37}$$

$$T_{zz} = -p_0 + \frac{\overline{\mu}_1}{B_1B_2} + \frac{c_0\mu_2}{\lambda_1^2\lambda_2^2} + \frac{2c_1\mu_2}{\lambda_1^4\lambda_2^4} = \frac{f_z}{a_0\lambda_1\lambda_2}, \tag{38}$$

where

$$\overline{\mu}_1 = \mu_1 + f'(N)(\lambda_2^4 - 1)^2.$$

After eliminating the Lagrangian multiplier p_0 from the above equations,

$$\begin{aligned} \bar{\mu}_1(B_2 - B_1) + c_0\mu_2(\lambda_2^2 - \lambda_1^2) + 2c_1\mu_2(\lambda_2^4 - \lambda_1^4) \\ + 2c_2(\lambda_2^2-1)\lambda_2^2 + 2c_3(\lambda_2^4-1)\lambda_2^4 = 0, \end{aligned} \tag{39}$$

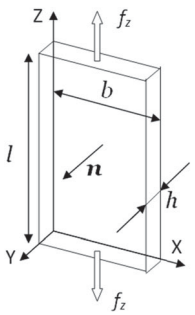

Figure 2. Composite specimen of dimensions $l \times b \times h$ subjected to cyclic uniaxial load f_z and **n** is the preferred direction.

$$\begin{aligned} \overline{\mu}_1\left(\frac{1}{B_1B_2} - B_1\right) + c_0\mu_2\left(\frac{1}{\lambda_1^2\lambda_2^2} - \lambda_1^2\right) \\ + 2c_1\mu_2\left(\frac{1}{\lambda_1^4\lambda_2^4} - \lambda_1^4\right) = \frac{f_z}{a_0\lambda_1\lambda_2}. \end{aligned} \tag{40}$$

In the above equations, f_z represents the loading history as a function of time and a_0 is the original area of cross-section.

The loading function is a sinusoidal excitation of the form (obtained from the experimental data of [20])

$$f_z = f_0 + \frac{a}{2}\sin(2\pi nt + \phi) \;\forall\, t > t_0. \tag{41}$$

In this equation, f_0 is the mean load, a is the load amplitude, n is the frequency of loading, ϕ is the initial phase and t_0 is the rise time during which ramp loading is applied. There are two sets of loading functions for which simulations were performed. The values of the parameters for these loading functions are noted in table 1.

From eqn. (29), we obtain three equations for evolution of strain, of which one is redundant. The remaining two equations are:

$$\begin{aligned} \dot{B}_1 = 2B_1\frac{\dot{\lambda}_1}{\lambda_1} + 2\left(\frac{\mu_1}{2v}\right)^{\frac{1}{2\beta-1}}\left(\frac{3B_1B_2}{B_1+B_2+B_1^2B_2^2} - B_1\right) \\ \left[B_1 + B_2 + \frac{1}{B_1B_2} - \frac{9B_1B_2}{B_1+B_2+B_1^2B_2^2}\right]^{\frac{1-\beta}{2\beta-1}}, \end{aligned} \tag{42}$$

and

$$\begin{aligned} \dot{B}_2 = 2B_2\frac{\dot{\lambda}_2}{\lambda_2} + 2\left(\frac{\mu_1}{2v}\right)^{\frac{1}{2\beta-1}}\left(\frac{3B_1B_2}{B_1+B_2+B_1^2B_2^2} - B_2\right) \\ \times \left[B_1 + B_2 + \frac{1}{B_1B_2} - \frac{9B_1B_2}{B_1+B_2+B_1^2B_2^2}\right]^{\frac{1-\beta}{2\beta-1}}. \end{aligned} \tag{43}$$

Equations (39), (40), (42) and (43) form a system of algebraic and differential equations in terms of $B_1, B_2, \lambda_1, \lambda_2$ and are solved numerically.

3. Results and discussion

The system of algebraic and differential equations were together solved numerically with necessary initial conditions (ICs). Since the material occupies the reference configuration at initial time, deformation gradient is set to identity tensor initially. The following ICs were used:

$$B_1(0) = B_2(0) = \lambda_1(0) = \lambda_2(0) = 1. \tag{44}$$

Table 1. Parameters of loading function.

$f_z = f_0 + \frac{a}{2}\sin(2\pi nt + \phi) \forall t > t_0$

	f_0 (kN)	a (kN)	n (Hz)	ϕ (rad)	t_0 (s)
Set1	29.061	10.1952	1	0.5918	100
Set2	30.564	10.6568	1	0.5918	100

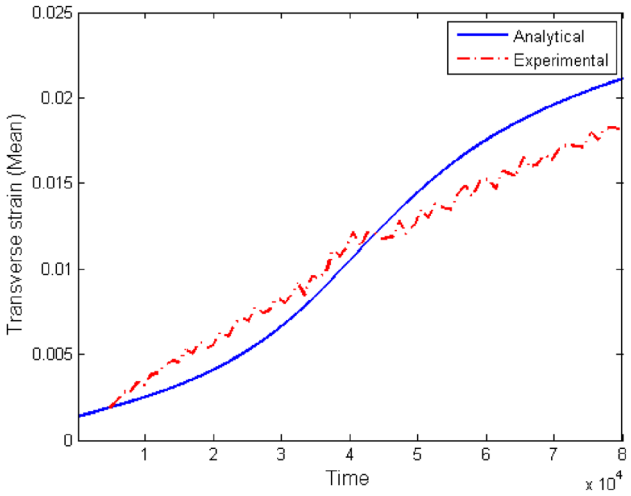

Figure 3. Mean of transverse strain (Set 1: 90% σ_{ult}).

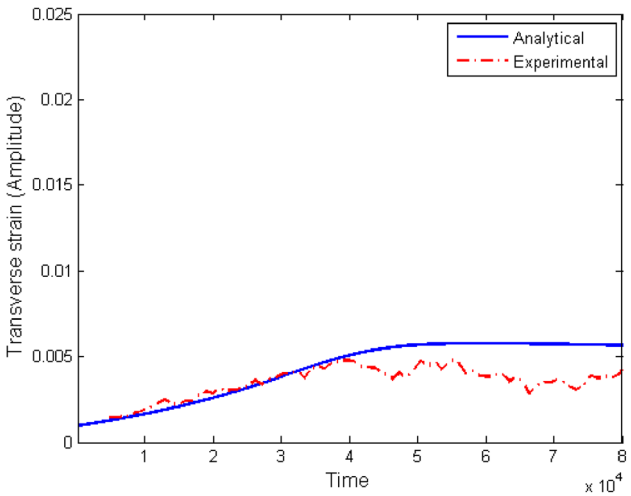

Figure 4. Amplitude of transverse strain (Set 1: 90% σ_{ult}).

The solutions were obtained using Euler's explicit scheme and the algebraic equations were solved using the Newton–Raphson method. The simulations were performed using MATLAB®. Stability and convergence were ensured. The code was checked for grid independence.

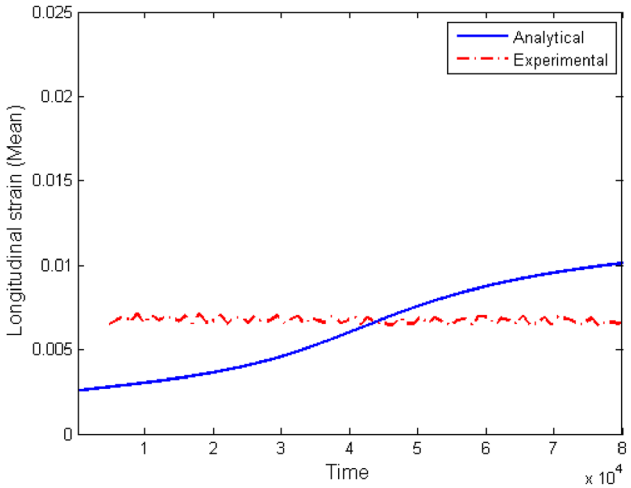

Figure 5. Mean of longitudinal strain (Set 1: 90% σ_{ult}).

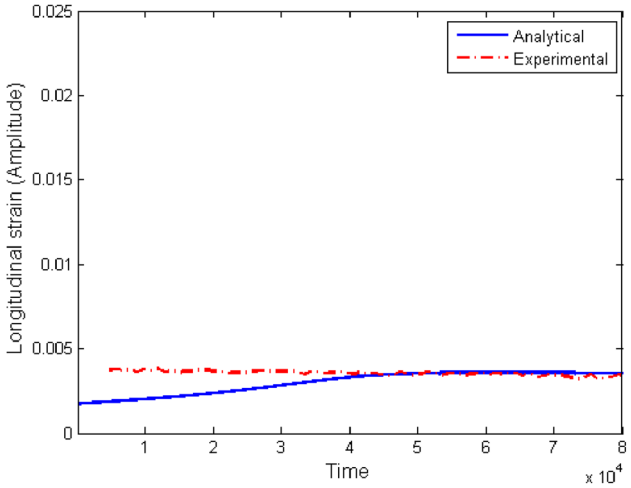

Figure 6. Amplitude of longitudinal strain (Set 1: 90% σ_{ult}).

The strains predicted by the model are compared against the average strain on the cross-section. The experimental data reported by Khaja Mohiddin *et al* [20] were used for this exercise. Figures 3, 4, 5 and 6 show the case of set 1 mentioned in table 1. Figures 7, 8, 9 and 10 show the case of set 2. The results show reasonable agreement with experimental data. The mean and amplitude of transverse strain over each cycle show a steadily increasing trend. The amplitude of transverse strain increases at first, due to softening in the material. However, the strain amplitude becomes fairly constant after a certain number of cycles. The variation in longitudinal strain is not as large as the transverse strain. This is indicative that damage in this case manifests first in the transverse direction. The model parameters corresponding to the results are given in table 2. The parameters were optimized using non-linear least-

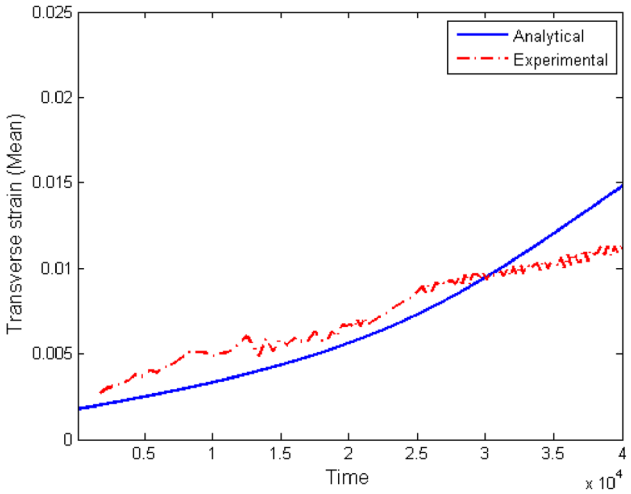

Figure 7. Mean of transverse strain (Set 2: 95% σ_{ult}).

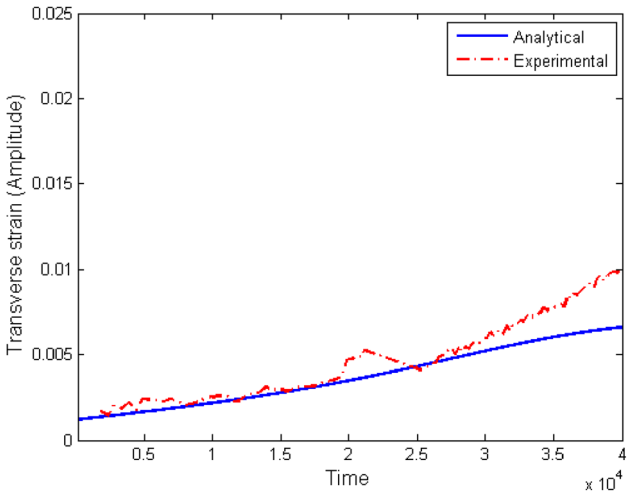

Figure 8. Amplitude of transverse strain (Set 2: 95% σ_{ult}).

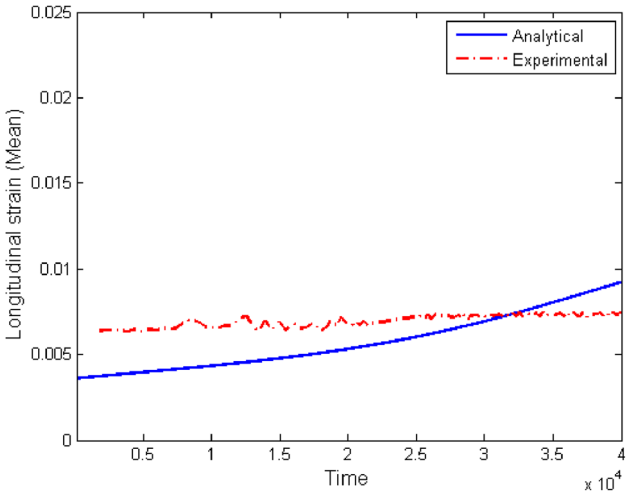

Figure 9. Mean of longitudinal strain (Set 2: 95% σ_{ult}).

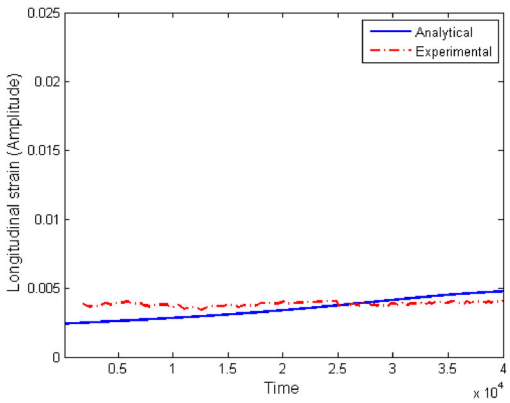

Figure 10. Amplitude of longitudinal strain (Set 2: 95% σ_{ult}).

squares method. The Gauss–Newton algorithm was used to solve the equations.

Hysteresis loops formed by load versus strain (figure 11) are plotted at different stages of loading cycles and compared with experimental data. The area under the hysteresis loop is initially small, but this area increases with time showing that dissipation becomes important over time.

4. Conclusion

A viscoelastic, homogeneous and incompressible constitutive model has been developed and used to model the behavior of CFRP composites in uniaxial cyclic loading. The composite laminate is treated as homogeneous, quasi-isotropic material and isothermal conditions are assumed throughout the loading cycles. The model was calibrated using experimental data. The study shows that the material response is close to elastic during the initial stages of cyclic loading. The longitudinal and transverse strains are captured reasonably well. The transverse strain is larger than the longitudinal strain which seems to be indicative that damage manifests first in the transverse direction. The energy dissipated by the material increases as the number of loading cycles increase. As the number of cycles increase, energy dissipation increases and dissipation becomes important.

Appendix I. Frame invariance of N

In eqn. (27), N is defined as, $N = \int_0^t \left| \mathbf{B}_{\kappa_{p(t)}}(\tau) \cdot \mathbf{D}(\tau) \right| d\tau$. It is required that N be frame invariant in order that the stress be frame invariant. For an observer 'A', the current

Table 2. Model parameters.

$c_3 = \frac{p}{(N+s)^r} + q$ where $N = \int_0^t \left\| \mathbf{B}_{\kappa_{p(t)}}(\tau) \cdot \mathbf{D}(\tau) \right\| \, d\tau$		
$\mu_1 = 1.03$ GPa	$\mu_2 = 5.56$ GPa	$v = 4988.1$ GPa · s
$\beta = 1$	$a_0 = 75$ mm^2	$c_0 = 1.65$
$c_1 = 1.15$	$c_2 = 2.0$	$p = 1.27$
$q = -14.5$	$r = 0.83$	$s = 0.03$

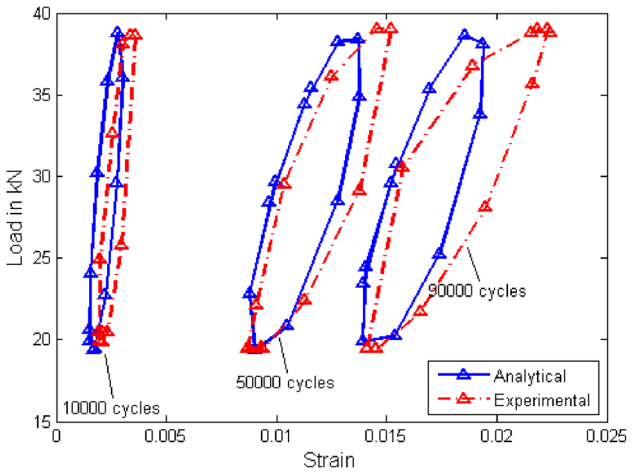

Figure 11. Load versus strain (hysteresis) at different stages of loading.

configuration is denoted as $\mathbf{x}_{\kappa_t}$. Consider another observer 'B' for whom the current configuration is denoted as $\mathbf{x}^*_{\kappa_t}$. The observers 'A' and 'B' are related through

$$\mathbf{x}^*_{\kappa_t} = \mathbf{Q}(t)\,\mathbf{x}_{\kappa_t} + \mathbf{c}(t), \tag{A1}$$

where $\mathbf{Q}(t)$ is a rotation tensor and $\mathbf{c}(t)$ is a translation vector.

Next, the transformation for certain kinematic quantities are shown below:

$$\mathbf{F}^*_{\kappa_R} = \frac{\partial \boldsymbol{x}^*}{\partial \boldsymbol{X}} = \frac{\partial \boldsymbol{x}^*}{\partial \boldsymbol{x}}\frac{\partial \boldsymbol{x}}{\partial \boldsymbol{X}} = \boldsymbol{Q}\boldsymbol{F}_{\kappa_R}, \tag{A2}$$

$$\boldsymbol{F}^*_{\kappa_{p(t)}} = \boldsymbol{Q}\boldsymbol{F}_{\kappa_{p(t)}}, \tag{A3}$$

$$\boldsymbol{B}^*_{\kappa_{p(t)}} = \boldsymbol{F}^*_{\kappa_{p(t)}}(\boldsymbol{F}^*_{\kappa_{p(t)}})^{\mathrm{T}} = \boldsymbol{Q}\boldsymbol{F}_{\kappa_{p(t)}}\boldsymbol{F}^{\mathrm{T}}_{\kappa_{p(t)}}\boldsymbol{Q}^{\mathrm{T}} = \boldsymbol{Q}\boldsymbol{B}_{\kappa_{p(t)}}\boldsymbol{Q}^{\mathrm{T}}. \tag{A4}$$

Differentiating (A2),

$$\dot{\mathbf{F}}^*_{\kappa_R} = \mathbf{Q}\dot{\mathbf{F}}_{\kappa_R} + \dot{\mathbf{Q}}\mathbf{F}_{\kappa_R} = \mathbf{Q}\mathbf{L}\mathbf{F}_{\kappa_R} + \dot{\mathbf{Q}}\mathbf{F}_{\kappa_R}, \tag{A5}$$

$$\begin{aligned}\mathbf{L}^* &= \dot{\mathbf{F}}^*_{\kappa_R}(\mathbf{F}^*_{\kappa_R})^{-1} = (\mathbf{Q}\mathbf{L}\mathbf{F}_{\kappa_R} + \dot{\mathbf{Q}}\mathbf{F}_{\kappa_R})(\mathbf{Q}\mathbf{F}_{\kappa_R})^{-1} \\ &= (\mathbf{Q}\mathbf{L}\mathbf{F}_{\kappa_R} + \dot{\mathbf{Q}}\mathbf{F}_{\kappa_R})\mathbf{F}_{\kappa_R}{}^{-1}\mathbf{Q}^{\mathrm{T}} = \mathbf{Q}\mathbf{L}\mathbf{Q}^{\mathrm{T}} + \dot{\mathbf{Q}}\mathbf{Q}^{\mathrm{T}},\end{aligned} \tag{A6}$$

$$(\mathbf{L}^*)^{\mathrm{T}} = \mathbf{Q}\mathbf{L}^{\mathrm{T}}\mathbf{Q}^{\mathrm{T}} + \mathbf{Q}(\dot{\mathbf{Q}})^{\mathrm{T}}. \tag{A7}$$

Adding (A6) and (A7),

$$2\mathbf{D}^* = 2\mathbf{Q}\mathbf{D}\mathbf{Q}^{\mathrm{T}} + \dot{\mathbf{Q}}\mathbf{Q}^{\mathrm{T}} + \mathbf{Q}(\dot{\mathbf{Q}})^{\mathrm{T}}. \tag{A8}$$

Since $\mathbf{Q}$ is orthogonal,

$$\mathbf{Q}\mathbf{Q}^{\mathrm{T}} = \mathbf{I}. \tag{A9}$$

Differentiating (A9),

$$\dot{\mathbf{Q}}\mathbf{Q}^{\mathrm{T}} + \mathbf{Q}(\dot{\mathbf{Q}})^{\mathrm{T}} = \mathbf{0}. \tag{A10}$$

Substituting (A10) in (A8),

$$\mathbf{D}^* = \mathbf{Q}\mathbf{D}\mathbf{Q}^{\mathrm{T}}. \tag{A11}$$

N is defined as,

$$N = \int_0^t \left\| \mathbf{B}_{\kappa_{p(t)}}(\tau) \cdot \mathbf{D}(\tau) \right\| d\tau = \int_0^t \left| tr(\mathbf{B}_{\kappa_{p(t)}}\mathbf{D})(\tau) \right| d\tau. \tag{A12}$$

For observer B, N^* would be,

$$N^* = \int_0^t \left| tr(\mathbf{B}^*_{\kappa_{p(t)}}\mathbf{D}^*)(\tau) \right| d\tau, \tag{A13}$$

and

$$\mathbf{B}^*_{\kappa_{p(t)}}\mathbf{D}^* = \mathbf{Q}\mathbf{B}_{\kappa_{p(t)}}\mathbf{Q}^{\mathrm{T}}\mathbf{Q}\mathbf{D}\mathbf{Q}^{\mathrm{T}} = \mathbf{Q}\mathbf{B}_{\kappa_{p(t)}}\mathbf{D}\mathbf{Q}^{\mathrm{T}}. \tag{A14}$$

Thus $\mathbf{B}^*_{\kappa_{p(t)}}\mathbf{D}^*$ is frame invariant. Hence $tr(\mathbf{B}^*_{\kappa_{p(t)}}\mathbf{D}^*)$ is also frame invariant as shown below:

$$\begin{aligned} tr(\mathbf{B}^*_{\kappa_{p(t)}}\mathbf{D}^*) &= tr(\mathbf{Q}\mathbf{B}_{\kappa_{p(t)}}\mathbf{D}\mathbf{Q}^{\mathrm{T}}) = tr(\mathbf{B}_{\kappa_{p(t)}}\mathbf{D}\mathbf{Q}^{T}\mathbf{Q}) \\ &= tr(\mathbf{B}_{\kappa_{p(t)}}\mathbf{D}). \end{aligned} \tag{A15}$$

Therefore,

$$N^* = \int_0^t \left| tr(\mathbf{B}^*_{\kappa_{p(t)}}\mathbf{D}^*)(\tau) \right| d\tau = \int_0^t \left| tr(\mathbf{B}_{\kappa_{p(t)}}\mathbf{D})(\tau) \right| d\tau = N. \tag{A16}$$

Since N^* is invariant for an arbitrary $\mathbf{Q}(t)$ and $\mathbf{c}(t)$, the value of N is independent of the frame of the observer.

Acknowledgements

The authors thank the Structures Panel of AR&DB for funding. The authors acknowledge the use of the computing resources at HPCE, IIT Madras.

References

[1] Epaarachchi J A and Clausen P D 2003 An empirical model for fatigue behavior prediction of glass fibre-reinforced plastic composites for various stress ratios and test frequencies. *Composites Part A* 34: 313–326

[2] Reifsnider K L and Talug A 1980 Analysis of fatigue damage in composite laminates. *Int. J. Fatigue* 2: 3–11

[3] Highsmith A L and Reifsnider K L 1982 Stiffness–reduction mechanisms in composite laminates. *Damage in Composite Materials: Basic Mechanisms, Accumulation, Tolerance, and Characterization*, ed. K. Reifsnider (West Conshohocken, PA: ASTM International) 103–117

[4] Yang J N 1978 Fatigue and Residual Strength Degradation for Graphite/Epoxy Composites Under Tension-Compression Cyclic Loadings. *J. Composite Materials* 12: 19–39

[5] Caprino G 1984 Residual Strength Prediction of Impacted CFRP Laminates. *J. Composite Materials* 18: 508–518

[6] Whitworth H A 2000 Evaluation of the residual strength degradation in composite laminates under fatigue loading. *Composite Structures* 48: 261–264

[7] Lin Y 1989 On fatigue damage accumulation and material degradation in composite materials. *Composites Sci. Tech.* 36: 339–350

[8] Guedes R M 2007 Durability of polymer matrix composites: Viscoelastic effect on static and fatigue loading. *Composites Sci. Tech.* 67:2574–2583

[9] Mao H and Mahadevan S 2002 Fatigue damage modelling of composite materials. *Composite Structures* 58: 405–410

[10] Mall S, Moschelle W R and Pernot J J 1993 Fatigue behavior of a fiber-reinforced ceramic matrix composite with a circular hole. *Composites Sci. Tech.* 49: 173–182

[11] Van Paepegem W, De Baere I, Lamkanfi E and Degrieck J 2007 Poisson's ratio as a sensitive indicator of (fatigue) damage in fibre-reinforced plastic. *Fatigue Fract. Eng. Mater. Struct.* 30: 269–276

[12] Van Paepegem W, De Baere I, Lamkanfi E and Degrieck J 2010 Monitoring quasi-static and cyclic fatigue damage in fibre-reinforced plastics by Poisson's ratio evolution. *Int. J. Fatigue* 32(1):184–196

[13] Akay E, Yilmaz C, Kocaman E S, Turkmen H S and Yildiz M 2016 Monitoring Poisson's Ratio Degradation of FRP Composites under Fatigue Loading Using Biaxially Embedded FBG Sensors. *Materials* 9(9):781. https://doi.org/10.3390/ma9090781

[14] Zhou G, Sun Q, Meng Z, Li D, Peng Y, Zeng D and Su X 2021 Experimental Investigation on the Effects of Fabric Architectures on Mechanical and Damage Behaviors of Carbon/Epoxy Woven Composites *Composite Structures* 257. https://doi.org/10.1016/j.compstruct.2020.113366.

[15] Khaja Mohiddin S M, Subramanian S J and Murthy H S N 2012 Study of damage evolution during fatigue of composites using DIC. *Proc. SEM XII International Congress and Exposition on Experimental and Applied Mechanics Conference*,Costa Mesa, USA

[16] Rajagopal K R and Srinivasa A R 2000 A thermodynamic frame work for rate type fluid model. *J. Nonnewton. Fluid Mech.* 88: 207–227

[17] Ramkumar A, Kannan K and Gnanamoorthy R 2010 Experimental and theoretical investigation of a polymer subjected to cyclic loading conditions. *Int. J. of Eng. Sci.* 48: 101–110

[18] Rao I J and Rajagopal K R 2002 A thermodynamic framework for the study of crystallization in polymers, *Zeit. ang. Math. Phys.* 53: 365–406

[19] Mollica F, Rajagopal K and Srinivasa A 2001 The inelastic beahavior of metals subject to loading reversal. *Int. J. Plasticity* 17: 1119–1146

[20] Khaja Mohiddin S M 2015 Fatigue damage characterization using digital image correlation. *MS thesis*, Dept. of Aerospace Eng., IIT-Madras, India.

[21] Rajagopal K R and Srinivasa A R 1998 Mechanics of the inelastic behavior of materials Part I. *Int. J. Plasticity* 14: 945–967.

[22] Green A E and Naghdi P M 1977 On thermodynamics and nature of the second law. *Proc. R. Soc. London A* 357: 253–270.